Performance Comparisons of FDD MIMO and 2.6 GHz TDD Massive MIMO: An Experimental Analysis

Engin Zeydan[1*], Omer Dedeoglu[2] and Yekta Turk[3]

[1] *Centre Technologic de Telecomunicacions de Catalunya, Castelldefels, Barcelona, Spain, 08860*

[2] *Türk Telekomünikasyon A.S. Istanbul, Turkey, 34889*

[3] *Mobile Network Architect Istanbul, Turkey, 34889*

Abstract

Massive multiple-input multiple-output (MIMO) is considered as a breakthrough technology in 5G and beyond 5G systems. Some of its main advantages are providing high spectral efficiency to many users simultaneously in the same time-frequency blocks, strong directive signals towards short-range areas and little interference leaks. However, while massive MIMO exhibits interesting benefits, it is important to investigate its main gains through real deployment scenarios in an operator's infrastructure. In this paper, we focus on performance comparisons of traditional frequency-division duplex (FDD)-based MIMO and 2.6 GHz Time-division duplex (TDD)-based massive MIMO deployments through experimental analysis under different spectrum and bandwidth in a total of three separate sites and one co-site in an operational infrastructure of an operator in Turkey. We also provide design guidelines and requirements for massive MIMO network deployment and proper acceptance of Key Performance Indicators (KPIs) collection and comparisons criteria. Our experimental results reveal up to 66%, 56% and 23% performance benefits in terms of downlink (DL) cell throughput of 2.6 Ghz TDD-based massive MIMO compared to FDD-based MIMO sites in 800 Mhz (site with approximately same number of User Equip-

*Corresponding author

Email address: engin.zeydan@cttc.cat (Engin Zeydan[1])

ment (UEs) compared with TDD massive MIMO), 1800 Mhz (site with higher number of UEs compared with TDD massive MIMO) and 2600 Mhz (site with lower number of UEs compared with TDD massive MIMO) respectively each having 10 Mhz bandwidth. On the other hand, LTE 1800 Mhz FDD MIMO at 20 Mhz can yield higher user throughput values in comparison to 2.6 GHz TDD-based massive MIMO at 10 Mhz. We also observed that the maximum paired layer reached 14 layers in DL of TDD-based massive MIMO. At the end of the paper, we address the main observations and takeaways of TDD-based massive MIMO deployments.

Keywords: Massive MIMO, experimental trials, TDD, FDD, cellular networks

1. Introduction

Cellular networks are experiencing exponential traffic growth recently. According to the Ericsson Mobility Report of June 2020, mobile traffic is expected to grow by 31 percent annually between 2019 and 2025 and most of it will be from video traffic [1]. Moreover, in the same report 5G networks are expected to carry nearly half of the world's mobile data traffic in 2025. Higher traffic brings together ultra dense cellular network deployments which also increase the total interference levels in the network. Interference still remains to be the major limitation of improving Spectral Efficiency (SE) in cellular networks. There have been many interfernce management techniques studied in both academia and industry. To circumvent the interference, higher frequencies are not the appropriate solution. As a matter of fact, higher frequencies can even increase the interference. On the other hand, it is known theoretically that the SE and hence data rate can grow with the number of antennas and users [2]. To achieve uniform coverage inside cellular networks, stronger signals with same interference levels at the cell coverage area are desired. This can be achieved with beamforming via multiple antennas. To achieve beamforming, the same signal needs to be transmitted from all antennas by either varying phase/amplitude per antenna or per user.

Massive Multiple Input Multiple Output (MIMO) ensures directed signaling by deploying beamforming antennas rather than traditional antennas to enhance energy efficiency as well as SE. The main characteristics of massive MIMO is that the number of antennas (transceiver chains) in the Base Stations (BSs) is larger than the number of users in the coverage area [3]. Together with massive MIMO, BSs can fully separate the users by providing favorable propagation environment for separate users [4]. It uses antenna arrays that are on a chip for easy beamforming and results in higher received power and spatial multiplexing. Antenna separations are also small. With few antennas, only broad beams can be achieved, whereas massive number of antennas (e.g. more than 200) results in many narrow beams (hence fewer multipath components), less leakage in undesired directions (good for urban neighborhoods) and main lobe to be focused on desired users. Together with more antennas, transmit power can be reduced and more simultaneous users can be multiplexed.

Experimental validations of massive MIMO are important to understand the gains in real-world scenarios. In this paper, we study the performance comparisons of 2.6 GHz Time-division duplex (TDD)-based massive MIMO scheme with different operating frequency Frequency-division duplex (FDD)-based MIMO schemes in an operational infrastructure of an operator in Turkey.

2. Related Work and Motivation

The major benefits from massive MIMO deployments has been shown in capacity and throughput improvements in many of the previous works [5, 3]. Thanks to its multiplexing and array gains, massive MIMO can also provide high SE (in bits/s/Hz). Massive MIMO based 5G networks is becoming a trending area of study in both academic and industry. Massive MIMO is converting into a practical technology to be used in operators' network infrastructure after its introduction ten years ago. It has emerged in many of the products of major vendors such as Nokia's AirScale, Ericsson's AIR and Huawei's AAU and is currently being deployed widely today by various operators (e.g. Sprint, TMO

in North America) across their LTE networks on a large scale. Massive MIMO is going to be a key enabler technology of 5G as well. At the same time, the basic principles of massive MIMO operation is going to be similar to Long Term Evolution (LTE). Additionally, 5G New Radio (NR) is optimized for massive MIMO design with additional features to support beamforming, advanced high spatial resolution codebooks for support up to 256 antennas, high resolution channel state information (CSI)-Reference Signal (RS) design and reporting mechanisms [6].

Massive MIMO is also foreseen as a promising enabler technology for 6G under the name ultra-massive MIMO [7]. The authors in [8] investigate the potential of massive MIMO in green communications. Large number of measurement campaigns have also been held for massive MIMO [9, 10, 11, 12, 13, 14, 15]. The authors in [9] provide a good overview of recent 5G experimental activities in massive MIMO. Some of the massive MIMO experimental campaigns include measurements on spectrum efficiency and capacity [10], channel to model channel matrix [11] and its characteristics [12], frequency-domain channel sounding [13], spectrum sensing in a cognitive radio-like network [14], channel hardening and user orthogonality in [15].

New trials are beginning to emerge converging 5G with massive MIMO technology. In 2019, US carrier Sprint (now T-Mobile) has completed 5G data usage via its 2.5 GHz massive MIMO BS working on 3GPP 5G NR [16]. In 5G trials, Ericsson and T-Mobile has demonstrated a 16-layer Multi User (MU)-MIMO trial to achieve peak cell throughput of more than 5.6 Gbps on one channel of 2.5 GHz spectrum and 50 bps/Hz SE with 100 Mhz of total 5G spectrum [17]. During this joint experiment, massive MIMO with 64 antennas are used that transmit 16 layers (unique data streams each capable of transmitting more than 35 Mbps). At the receiving end, eight smartphones that are using the same radio resource simultaneously were used with each capable of receiving two data streams, i.e. 2-layers (which totals to 700 Mbps per device). In terms of comparisons of FDD and TDD massive MIMO, e.g. based on data obtained in measurement campaigns, the authors in [18] have compared TDD based massive

MIMO with four flavors of FDD beamforming distinguished based on feedback of CSI using the channel measurements at 2.6 Ghz. Extensive measurements at 3.5 GHz using a sounding system that captures the dynamic channels towards users are also used to compare different precoding schemes for TDD and FDD massive MIMO systems in [19].

Various deployment options for massive MIMO are also proposed in both academia and industry perspectives [20]. For indoor massive MIMO deployments, standalone massive MIMO at a single location, distributed MIMO without cooperation, and network MIMO with full cooperation are available in the literature [21]. Traditional massive MIMO BSs does not cooperate. For outdoor, single, cluster or city deployments are possible in practice. In cluster deployments, typically a number of sites on the order of tens is allocated to a cluster so that managing and tuning the cluster becomes easier.

On the other hand, in Downlink (DL) MIMO side, The 3rd Generation Partnership Project (3GPP) has defined various Transmission Modes (TMs) to be used in LTE and in 5G with beamforming options. The white paper in [22] provides a good overview of LTE TMs and beamforming used in MIMO technologies. As defined in 3GPP Release 15 [23, 24], TM7 to TM9 are used in 5G NR. Besides, TM3 to TM6 use codebook based precoding and TM7 to TM9 use non-codebook based precoding in LTE.

Some recent advances such as cell-free massive MIMO systems have also been proposed as a core architecture of the next-generation mobile communication networks [25, 26, 27, 28]. Cell-free massive MIMO aims to overcome the physical limitations (e.g. inter-cell interference) of traditional cellular networks. It is also shown to save more downlink transmission power than co-located massive MIMO systems [28]. An aerial intelligent reflecting surface assisted cell-free massive MIMO system to reduce the so-called "shadow areas" limitations of cell-free massive MIMO systems is proposed in [27]. At the same time, there are investigations that aim to realize the implementation of cell-free massive MIMO systems via radio stripes [25]. However, raising scalability issues due to increased network size brings higher computation complexity and demanding

fronthaul requirements. Hence, this problem needs to be handled appropriately in real-world implementations of cell-free massive MIMO systems [26].

Theoretical and simulation results are some of the main works that are studied in the literature of massive MIMO. However, as far as the authors are aware of, no detailed works on real-world experimental validations for comparisons between TDD-based massive MIMO and traditional FDD-based MIMO scenarios with different bandwidth utilizations using an operator's infrastructure has been attempted before in the literature. Similar to the experiments performed in this paper, in our previous study of [5] we investigated an experimental analysis of a massive MIMO trial focusing on TDD-based deployment using one of the telecommunication operator's infrastructure over a commercial site based in Turkey. However, the study in [5] did not investigate the effect of different carrier/operating frequencies on the performance of FDD based MIMO in comparison with TDD-based massive MIMO and lacks design guidelines and requirements for successful deployment of massive MIMO. This paper extends the previous study by providing a comprehensive performance comparison analysis under different operating frequencies under both co-site and separate FDD based MIMO deployments with different load characteristics.

Main Contributions: In this paper, we study TDD-based massive MIMO deployment trial inside the commercial infrastructure of a telecommunication operator in Turkey. More specifically, our focus has been on comparisons of TDD-based massive MIMO deployment with co-site and separate FDD-based MIMO deployments under different operating frequencies. Our comparisons are done via observing several operator specific Key Performance Indicators (KPIs). The main contributions of the paper can be summarized as follows:

- A real world experimental trial on a commercial site in Turkey for monitoring the performance differences of 2.6 GHz TDD-based massive MIMO with a total of four different sites FDD-based MIMO deployments that are under different operating frequency and bandwidth.
- Revealing up to 66%, 56% and 23% performance benefits in terms of DL

cell throughput of 2.6 Ghz TDD-based massive MIMO compared to FDD-based MIMO sites in 800 Mhz (site with approximately same number of user equipments (UEs) compared with TDD massive MIMO), 1800 Mhz (site with higher number of UEs compared with TDD massive MIMO) and 2600 Mhz (site with lower number of UEs compared with TDD massive MIMO) respectively for 10 Mhz bandwidth. On the other hand, LTE 1800 Mhz FDD MIMO at 20 Mhz can also yield higher user throughput values in comparison to 2.6 GHz TDD-based massive MIMO at 10 Mhz.

- Providing design guidelines and requirements for massive MIMO network deployment and proper acceptance of KPIs collection and comparisons criteria.

- Addressing main takeaways of the experimental results and the possible trade-offs of massive MIMO deployments.

The rest of the paper is organized as follows: In Section 3, we detail the system model, concepts, utilized metrics and practical settings and requirements for massive MIMO deployment. In Section 4, we provide our experimental results and point out some of the main outcomes of the conducted experimental scenarios. Finally in Section 5 we give the conclusions and future work of the paper.

Notation: The mathematical notations $\mathbf{X}$, $\mathbf{x}$ and x denote a generic matrix, vector and scalar respectively, $\mathcal{C}^{N\times M}$ denotes the set of complex valued $N \times M$ matrices, $\mathbf{A}^H$ is the conjugate transpose of matrix $\mathbf{A}$, $\mathcal{CN}(x, X)$ is the complex Gaussian distribution with mean x and covariance matrix X.

3. System Model and Concepts

We consider the DL of a cellular network as given in Figure 1. We assume that the access network involves one massive MIMO BSs and each equipped with M antennas. There are K UEs with N antennas where M is much larger than K to leverage the array gain in massive MIMO, which are spatially multiplexed

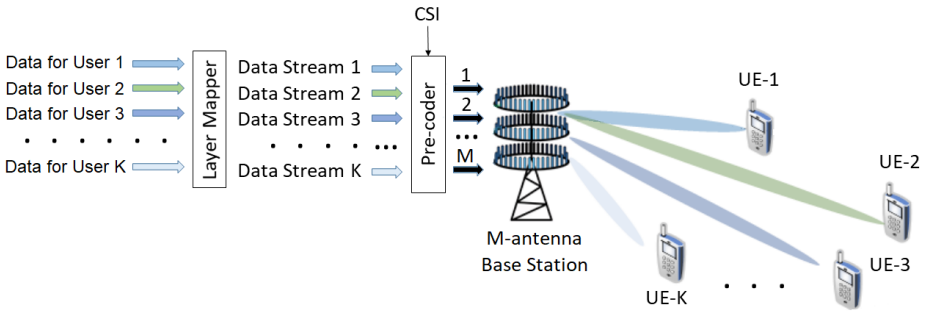

Figure 1: An illustration of a massive MIMO system with layer mapping and precoding operations.

onto the same time-frequency resource, i.e. each time–frequency Resource Block (RB) of BS serves the K UEs simultaneously. As the number of antennas in the system increases, each UE will benefit from a separate wireless channel with high channel gain and low interference [29]. For FDD based MIMO systems, we consider the DL of 3GPP Rel. 15 system. In our FDD systems, all BS sectors and UEs are equipped with M_{FDD} antennas.

Figure 1 gives an illustration of a typical DL massive MIMO system in which each user data (user data 1 up to user data K) is passed into layer mapping where data is mapped to one or multiple layers. Later, multiple data streams (data stream-1 up to data-stream K) are precoded with CSI and transmitted to intended UEs simultaneously by the M antennas massive MIMO BS. At each time instant [t], the transmitter applies a pre-coder to the $KN \times 1$ data vector $\mathbf{s}[t]$ that is intended for the K UEs. The $KN \times 1$ data vector $\mathbf{s}[t]$ is the stacking of the $N \times 1$ vectors $s_k[t] = [s_{k,1}[t], s_{k,2}[t], \ldots, s_{k,N}[t]]^T$ of the K UEs users where each entry is the data point from the a modulation constellation. During precoding, a precoding matrix $\mathbf{W}$ is applied and the transmitted $M \times 1$ data vector $\mathbf{x}[t]$ can be described by

$$\mathbf{x}[t] = \mathbf{W}^H \mathbf{s}[t] \tag{1}$$

where the $KN \times M$ matrix $\mathbf{W}$ contains the parameters of all channel elements, $\mathbf{s}[t]$ represents $KN \times 1$ data vector intended for the K UEs.

The received signal at k-th UE is collected in an $N \times 1$ vector $\mathbf{r}_k[t] = [r_{k,1}[t], r_{k,2}[t], ..., r_{k,N}[t]]^T$ and is given by

$$\mathbf{r}_k[t] = \mathbf{H}_k^T \mathbf{x}_k[t] + \mathbf{n}_k[t] \tag{2}$$

where $\mathbf{x}_k[t]$ is the $M \times 1$ pre-coded data vector, the elements $h_{m,n}^k$ of the $M \times N$ channel matrices $\mathbf{H}_k$ are the complex channel gains from the m-th transmitting antenna to the n-th receiving antenna and $N \times 1$ vector $\mathbf{n}_k \sim \mathcal{CN}(0, \sigma_{DL}^2 \mathbf{I})$ is the independent additive receiver noise with variance σ_{DL}^2 and $\mathbf{I}$ is the $N \times N$ identity matrix for k-th UE.

3.1. TDD and FDD MIMO systems

The transmission in MIMO systems can be done either in TDD or FDD mode. In FDD systems, Uplink (UL) and DL use different frequency bands but in same time, hence have different CSI in UL and DL. TDD systems, UL and DL use the same frequency bands but at different times. It is generally assumed that the UL and DL channels are reciprocal, i.e. they are the same in TDD systems.

In most of the classical wireless systems and deployments, FDD based deployments are operating, whereas TDD-based deployments is beginning to be in use as a candidate system with the introduction of massive MIMO systems. FDD based MIMO and TDD based massive MIMO systems have their own characteristics, benefits and bottlenecks. As the number of antennas in BS increases, CSI estimation in FDD systems becomes near impossible, incurring a huge training overhead which reduces the SE of the network. To solve for CSI acquisition problem in FDD MIMO systems, two main categories based on either coding (e.g. [30]) or neural network approaches (e.g. [31]) are proposed. However, in TDD systems channel estimation overhead is independent of the number of BS antennas. In TDD mode, UE can transmit the pilots at the same frequency in both UL and DL directions to estimate the channel and later determine the best beam to be selected and increase the beam accuracy. Hence, TDD systems become more tolerable due to channel reciprocity that requires

only UL CSI to be estimated. Therefore, TDD-based massive MIMO is more favorable than FDD-based massive MIMO [5].

Conventional MIMO systems: In these systems, BSs serve multiple users and average power per unit service area is distributed homogeneously. In these systems both BSs and UEs have multiple antennas and antenna ports where multiple data streams are transmitted simultaneously using the same time/frequency resources. For example, in case of 2×2 MIMO and 4×4 MIMO, the peak throughput of a single UE can be doubled and quadrupled respectively. In MU MIMO case, the BS sends multiple data streams for each UEs again utilizing the same time-frequency resources.

TDD-based massive MIMO: Due to channel hardening (because of sufficient randomness and many antennas), almost no channel quality variations are observed in massive MIMO systems. Scheduling is also seldom needed in case of variations in user load and is left as optional which means that advanced scheduling algorithms may not provide the desired gains [32]. Cell-edge performance is also improved by a factor of number of antennas. On the other hand, pilot contamination (degrading system performance), time reciprocity assumption (can potentially break), increased computational complexity with precoder design, CSI estimation requirements (in case of large number of transmit antennas), scheduler design (if the number of users becomes more than the number of antennas), signal detection challenges and hardware cost (due to large number of antennas) are some examples of bottlenecks for TDD-based massive MIMO implementation [33].

A good comparison of multi-antenna transmission modes using Single User (SU), MU and massive MIMO with FDD and TDD strategies is provided in our previous work [5].

3.2. Utilized Metrics

In this subsection, we give the definitions of some of the utilized metrics namely, Radio Resource Control (RRC) setup success rate, E-UTRAN Radio Access Bearer (E-RAB) setup success rate, user throughput, cell throughput,

Channel Quality Indicator (CQI) and cell capacity.

In closed loop MIMO systems, a UE periodically report back its dedicated CQI reports that contain information on CQI values, Precoding Matrix Index (PMI) and Rank Indicator (RI). CQI value represents the most spectrally efficient Modulation Coding Scheme (MCS) that can be supported by the DL channel without exceeding a target Block Error Rate (BLER). The capacity of a cellular network in a given area which is measured in bps/km^2 can be be calculated as

$$C = B[Mhz] \times D[cells/km^2] \times SE[bps/Hz/cell] \tag{3}$$

where B is the available spectrum, D is the average cell density, and SE is the per-cell SE which represents the amount of information transferred per second over a unit bandwidth [34]. The SE measures simply the bits per Physical Resource Block (PRB) in Hz and is calculated as UL cell throughput in bits divided by number of PRBs used by Physical Uplink Shared Channel (PUSCH) dedicated radio bearer per msec, RB in Hz and number of UL antennas [5]. In practical LTE deployment scenarios, signal-to-interference-plus-noise ratio (SINR) values are first mapped into CQI and later into SE using 3GPP specification tables (see Table 7.2.3-1 in [35]). Finally, it loops through MCS indexes to find the best Transport Block Size (TBS)- MCS pair that can approximate the obtained spectral efficiency and maps an MCS index into a TBS (see Table 7.1.7.1-1 in [35]) during one Transmission Time Interval (TTI).

DL average user throughput considers user throughput values and DL average cell throughput measures cell capacity. RRC setup success rate KPI simply measures successful attachment counts of UEs into the network during RRC connection request of UEs which can be formulated as

$$RRCSetUp_{SR} = \frac{\#\text{ of } RRCSetUpSuccess}{\#\text{ of } RRCSetUpAttempt} \times 100\% \tag{4}$$

where $RRCSetUpSuccess$ is RRC connection establishment's success count and $RRCSetUpAttempt$ is RRC connection establishments attempt count. After successful RRC connection, the network goes from RRC_idle mode to $RRC\_connected$

mode. Some possible practical reasons for observing low RRC setup success rates in a call are related to resource allocation failure (due to UE admission failures) or no response from UE (due to poor coverage or terminal problem) [36].

An E-RAB carries the service data of UEs as an access layer bearer. E-RAB setup success rate is related to accessibility and E-RAB counter KPI is utilized after successful RRC connection. The E-RAB success rate depends on successful connections to Core Network (CN) which can be formulated as

$$ERABSetUp_{SR} = \frac{\#\text{ of } ERABSetUpSuccess}{\#\text{ of } ERABSetUpAttempt} \times 100\% \tag{5}$$

where $ERABSetUpSuccess$is successful E-RAB establishments and $ERABSetUpAttempt$ is received E-RAB establishment attempts [36].

3.3. Practical Settings and Requirements for massive MIMO deployment

In general, operators want to deploy massive MIMO for capacity improvements over their current LTE infrastructure without major degradation over their other operating networks. In case a problem is detected in some problematic sites, a lot of effort and involvement of network experts are required to identify the reasons for degraded KPIs. Performance improvements of massive MIMO is site-dependent that depends on various factors such as traffic loads and user distribution. In a typical massive MIMO deployment scenario, the number of nodes can vary, e.g. from one site (busy site) to one hundred (in city wide deployments). For this reason, enhancing capabilities of different cells based on cell behavior and potential performance expectations are critical. For large scale deployments, testing no performance degradation to existing network infrastructure after the introduction of massive MIMO can be costly. Multiple tools and drive test results are also necessary for this purpose. Therefore, an integrated approach to correlate data from configuration management, performance management, fault management, performance management or counters is needed so that before and after performance can be provided to resolve any issues. For this reason, a clear set of requirements and acceptance criterias should

be set before and after massive MIMO deployment. Some of those requirements that are needed for KPI performance acceptance are:

1. Selecting the set and number of performance KPIs to be collected, tracked before and after massive MIMO deployment at cell/cluster/network level
2. Selecting the time period for KPI data collection before and after massive MIMO deployments, i.e. for pre-check and post-check respectively. Normally, two weeks for pre-check and ten days for pro-check would be sufficient. Moreover, the time duration samples for each KPIs should be large enough to have enough samples to be analyzed. At least one hour of data collection per KPI would be sufficient.
3. Deciding on a well-defined schema of the collected KPI data (for both pre and post operations) for persistent storage which will help in easy access and analytics operations at later stages.
4. Aggregating the KPI samples according to user needs, e.g. daily, weekdays only, busy hour, user defined customized, etc.
5. Displaying the cell/cluster/network level on geographic maps and visualizing the collected KPIs as a daily trend visualization so that in any poor performance results, operators can decide the reasoning based on some transient or some local event.

After massive MIMO deployments, pre and post KPI data are compared to observe the main gains of the deployment. Additionally, post KPI data are compared with the pre-defined KPI targets. For KPI comparisons, average KPI value of the baseline period can be compared with the average KPI value after massive MIMO deployments including the standard deviations or confidence values (if number of samples or days to be included into the analysis for more fair comparisons as in [37]).

4. Experimental Results

4.1. Details of the Experimental Setup

We compare the system performance of TDD-based Massive MIMO scheme with conventional FDD-based SU-MIMO schemes by means of extensive experimental trials over the commercially available sites given in Fig. 2 that consists of a total of four sites with three sectors per site. Fig. 2 shows the locations of experimental three sites with FDD based MIMO (site-1, site-2 and site-3) together with co-sites having both TDD-based massive MIMO and FDD based MIMO in the middle of the map. TDD-based massive MIMO operates @2.6 GHz with 64T64R, $M = 64$ (using 10 Mhz bandwidth) and co-site's FDD-based MIMO operates @800 MHz (using 10 Mhz bandwidth) and @1.8 GHz (over 20 Mhz bandwidth) with 2T2R $M_{FDD} = 2$. Site-1 in Fig. 2 operates FDD @800 Mhz, site-2 operates FDD @1800 Mhz and site-3 operates FDD 2600 Mhzh each with 2T2R and 10 Mhz bandwidth. Table 1 shows the experimental parameters and their corresponding values used in our TDD massive MIMO experiments. We used TM9 capable UEs of LTE Release 10 during the experimental tests with massive MIMO. In order to evaluate results better in the considered LTE scenarios, we chose similar traffic and CQI condition FDD cells for fair performance comparisons.

4.2. Massive MIMO main KPIs

Fig. 3 shows some of the main KPIs that are observed during the observation duration of massive MIMO deployment. The investigated KPIs are

- **Access KPIs:** RRC set-up success rate (%), E-RAB set-up success rate (%),
- **User throughput KPIs:** DL user throughput (Mbps), DL average paired layers,
- **Channel Quality**: Rank I CQI, average CQI,

Figure 2: Locations of experimental sites in Turkey with 2 external FDD based MIMO sites (site-1 (800 Mhz band), site-2 (1800 Mhz band) and site-3 (2600 Mhz band)) all operating in 10 Mhz bandwidth and co-sites with TDD-based massive MIMO and FDD based MIMO (800 Mhz band and 10 Mhz bandwidth, 1800 Mhz band and 20 Mhz bandwidth).

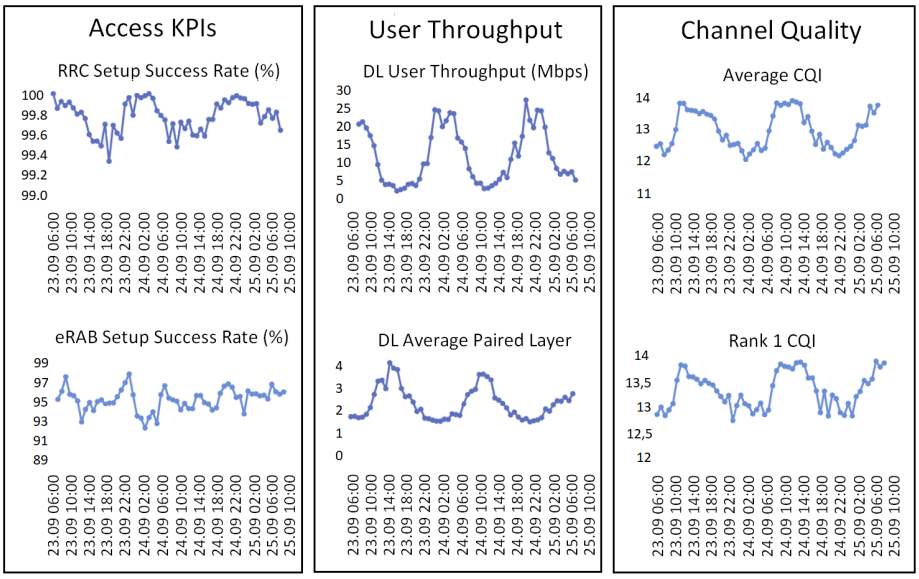

Figure 3: TDD-enabled massive MIMO BS KPI values for access, user throughput and channel quality.

Table 1

Experimental network parameters and their corresponding values used in TDD-based massive MIMO and FDD-based MIMO trials.

Parameter	**Value**	**Parameter**	**Value**
RAT	LTE TDD (Massive MIMO site) and FDD (MIMO sites)	UE category	TM-9 capable UEs of LTE Rel. 10
Carrier Frequency	2575 - 2615 MHz (2.6GHz B38)	Receiver noise power	-112 dBm
Number of subcarriers	600	Subcarrier bandwidth	15 kHz
Cyclic prefix overhead	6.67%	Frame dimensions	10 ms
Tx Power	40W	Occupied Bandwidth	10 Mhz
Antenna Config. (massive MIMO)	2 × 20 Mhz 64T64R	Transmission Scheme	OFDM
Antenna Height	28 meters	Mechanical Tilt	0 degrees
Electrical Tilt	1 degrees	Azimuth	310 degrees (D 220,G 340)
Scheduling algorithm	Proportional-fair	Instantaneous BandWidth (IBW)	40 Mhz
Common Public Radio Interface (CPRI) port number	2	CPRI Port Rate	100 Gbps
CPRI based topology	trunk	Max. distance from BBU	10 km
Dimensions (massive MIMO) (H x W x D)	860 mm x 520 mm x 170 mm	Dimensions (FDD MIMO) (H x W x D)	1509 mm x 469 mm x 206 mm
Polarization mode (FDD MIMO and TDD massive MIMO)	+45° and –45°	Gain (massive MiMO)	center downtilt: 16.3 dBi all downtilts: 16.1±0.7 dBi
Number of supported RF channels (massive MIMO)	64	Capacity (massive MIMO)	max. 3 carriers
Cross polar isolation (dB)	≥ 28	Antenna Spacing	λ / 2
Interband isolation (dB)	≥ 26	Impedance (Ω)	50
Gain (FDD MiMO) at mid Tilt	14.0 dBi (800 Mhz), 16.7 dBi (1800 Mhz), and 17.6 dBi (2600 Mhz)		

From access KPIs' perspective, Fig. 3 shows that both RRC setup success rate and E-RAB setup success rate values are above 99.4% and 93% respectively. Hence, we can conclude that RRC and E-RAB setup success rates have been relatively stable after the activation of TDD-based massive MIMO. From Fig. 3, we can also observe that channel quality values are in general good. Average CQI values are between 12 and 14 and rank-1 CQI values are slightly better and seldom drop below 13. Note that the values for the rank-1 CQI indicate the single CQI feedback values reported by UEs [38].

4.3. Massive MIMO Traffic

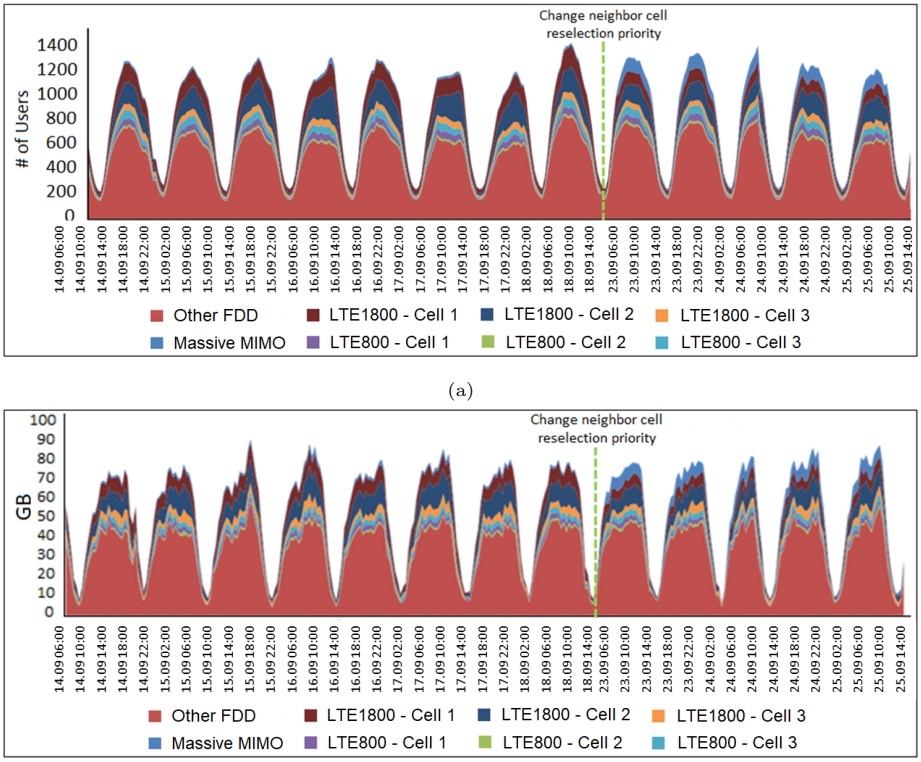

(a)

(b)

Figure 4: Overall performance analysis among all test sites (co-site and site-1, site-2 and site-3) (a) User distribution (b) PS traffic distribution.

Fig. 4 shows the overall user and PS traffic distributions among co-site and

other FDD MIMO sites. First of all, we can observe the period behavior of a number of users and throughput where the peak hours are reached around noon time and low periods of traffic are observed in the early morning. The pre-check period. i.e. before massive MIMO deployment observation duration, is selected to be 5 days (from 14 September 2018 to 18 September 2018) and post-check period, i.e. after massive MIMO deployment observation duration, is selected to be 3 days (from 23 September 2018 to 25 September 2018). Each measurement is collected and averaged over one hour time intervals. In Fig. 4, other FDD represents the total number of UEs and total Packet Switched (PS) traffic in site-1, site-2 and site-3 of Fig. 2. LTE 800 Mhz (having 10 Mhz bandwidth) and LTE 1800 Mhz (having 20 Mhz bandwidth) cells represent the co-site's number of UEs and PS traffic values. Note that the number of UEs and PS traffic does not change much over the course of pre-check and post-check periods over other FDD sites.

After changing neighbor cell re-selection priority at FDD co-site to migrate UEs from FDD to TDD massive MIMO enabled co-site, more LTE users are switched into TDD-based massive MIMO network. Therefore, we can observe that TDD users mainly migrated from co-site LTE 1800 Mhz cells (namely cell-1 and cell-2) after changing the cell re-selection priority. Fig. 5(a) and Fig. 5(b) show the FDD DL PRB utilization values after re-selection priority. We can observe that FDD DL PRB used ratio has decreased in both co-sites. Hence, the massive MIMO TDD site has absorbed the traffic from its FDD LTE 1800 Mhz co-site. Additionally, we can also infer that since higher signal strength and coverage are provided in the serving area with the TDD-based massive MIMO network, more UEs previously on cell-edge has more probability of being in the coverage of the site now.

4.4. Performance comparisons for different number of UEs

In this subsection, we compare TDD-based massive MIMO with FDD at 10 Mhz bandwidth with the different number of UEs in the system in Fig. 6, Fig. 7 and Fig. 8. First of all, we can observe from those figures that in terms of

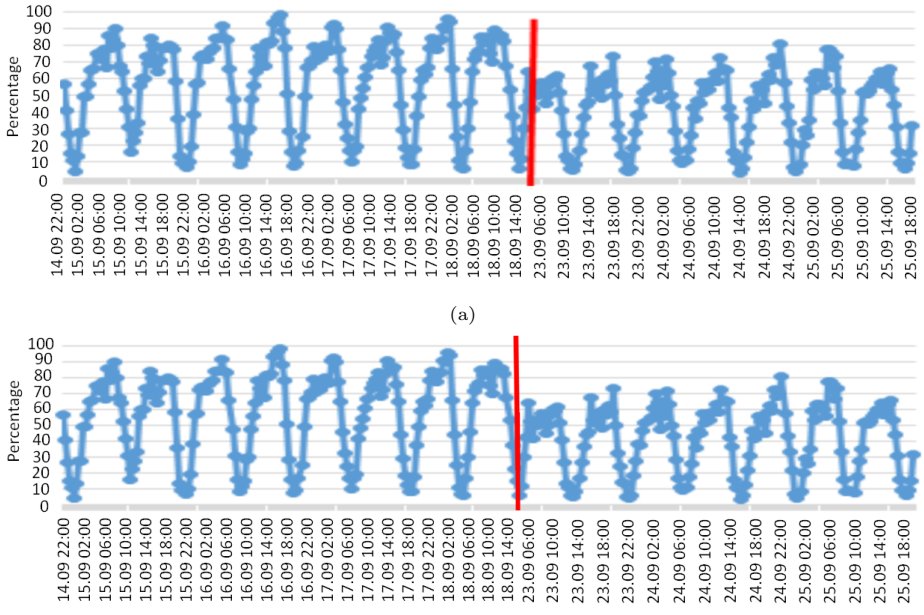

(a)

(b)

Figure 5: PRB utilization percentages of LTE 1800 FDD co-site after massive MIMO activation on (a) Cell-1 (b) Cell-2.

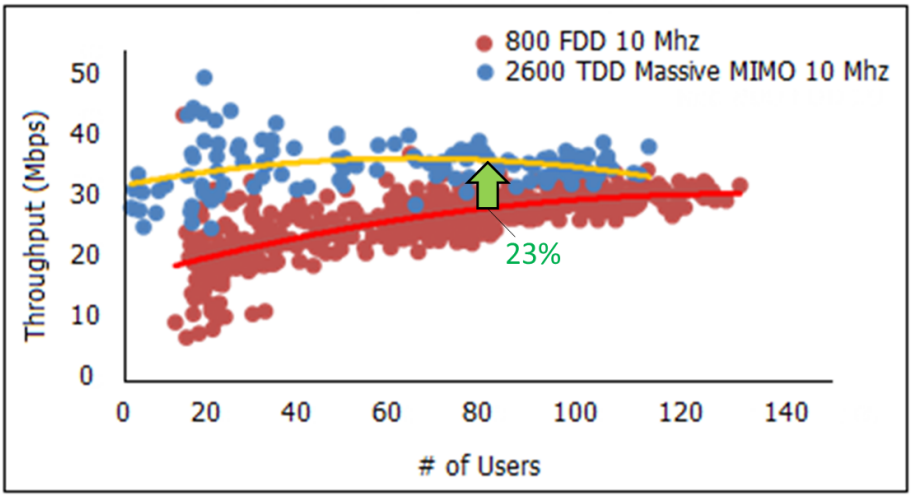

Figure 6: Cell throughput performance comparisons FDD 800 Mhz with 10 Mhz bandwidth v.s. 2600 Mhz TDD Massive MIMO with 10 Mhz bandwidth at site-1.

distribution of number of UEs in the coverage area, site-1 exhibits almost the same behavior with TDD-based massive MIMO, site-2 has higher number of UEs and site-3 has less number of UEs in comparisons to TDD-based massive MIMO.

Fig. 6 shows the scatter plot for MIMO experimental test results comparisons of DL cell throughput of FDD 800 Mhz with 10 Mhz bandwidth and 2600 Mhz TDD Massive MIMO with 10 Mhz bandwidth versus the number of UEs on the site-1's commercial user traffic on X-axis. In this figure, the yellow colored line represents the fitted regression line for TDD-based massive MIMO case whereas the red colored line represents the fitted regression line for FDD-based MIMO case. The number of UEs in TDD case has exceeded little above 120 UEs whereas it is a little below 120 UEs in FDD scenario. We can observe from Fig. 6 that TDD-based massive MIMO with 10 Mhz bandwidth yields approximately 23% improvements when number of UEs is around $K = 80$ compared to FDD-based MIMO in 10 Mhz bandwidth. This shows the clear advantage of TDD-based massive MIMO compared to FDD-based MIMO under the same bandwidth.

Fig. 7 shows the scatter plot of cell throughput performance comparisons between FDD 1800 Mhz with 10 Mhz bandwidth and 2600 Mhz TDD Massive MIMO with 10 Mhz bandwidth as the number of UEs is increasing in X-axis of site-2. In this figure, the yellow colored line represents the fitted regression line for TDD-based massive MIMO case whereas the red colored line represents the fitted regression line for FDD-based MIMO case. In this case, the number of UEs is close to 300 UEs in FDD scenario and it is the same distribution as in Fig. 6 for TDD-based massive MIMO. Fig. 7 shows that TDD-based massive MIMO with 10 Mhz bandwidth yields approximately 56% improvement when number of UEs is around $K = 100$ compared to FDD-based MIMO in 10 Mhz bandwidth. This again validates the clear advantage of TDD-based massive MIMO compared to FDD-based MIMO under same bandwidth. In comparison with the improvements in Fig. 6, Fig. 7 shows that increased frequency for FDD system has degraded the system performance.

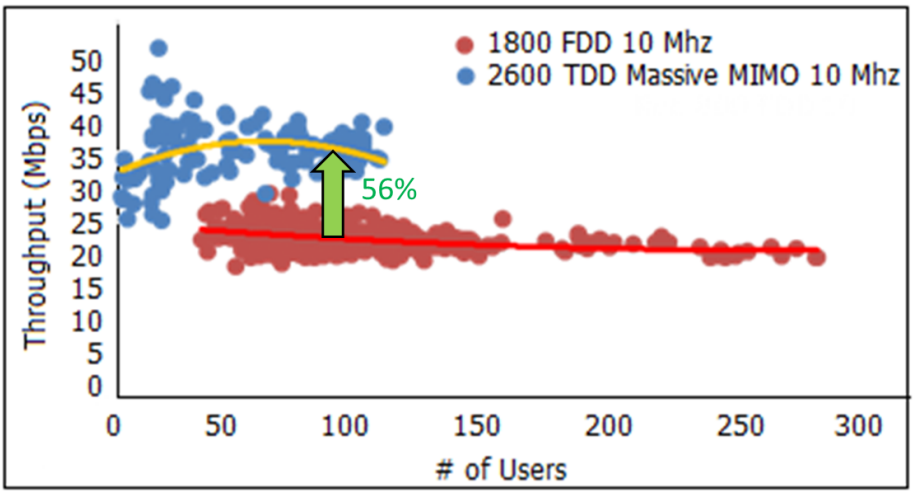

Figure 7: Cell throughput performance comparisons FDD 1800 Mhz with 10 Mhz bandwidth vs.2600 Mhz TDD Massive MIMO with 10 Mhz bandwidth at site-2.

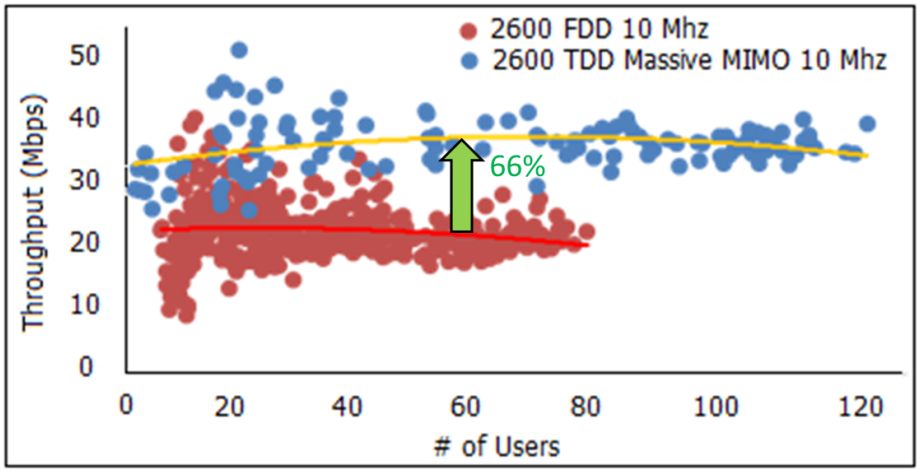

Figure 8: Cell throughput performance comparisons FDD 2600 Mhz with 10 Mhz bandwidth vs.2600 Mhz TDD Massive MIMO with 10 Mhz bandwidth at site-3.

Fig. 8 shows the scatter plot results of DL cell throughput performance comparisons FDD 2600 Mhz with 10 Mhz bandwidth versus 2600 Mhz TDD Massive MIMO with 10 Mhz bandwidth in Y-axis and the number of UEs on the site-3's commercial user traffic in X-axis. In this figure, the yellow colored line represents the fitted regression line for TDD-based massive MIMO case whereas the red colored line represents the fitted regression line for FDD-based MIMO case. The number of UEs in FDD scenario reaches up to 80 UEs whereas it goes up to 120 UEs in TDD cases. We can observe from Fig. 8 that TDD-based massive MIMO with 10 Mhz bandwidth yields approximately 66% improvement when number of UEs is around $K = 60$ compared to FDD-based MIMO in 10 Mhz bandwidth. This shows again the clear advantage of TDD-based massive MIMO compared to FDD-based MIMO under the same bandwidth and degradation effect of high frequency in FDD system.

Note that when comparing Fig. 6, Fig. 7, and Fig. 8, we can observe that as the number of users increase, sometimes FDD-based MIMO achieves better cell throughput than TDD Massive MIMO, and sometimes it does not. As a matter of fact, cell throughput depends on various factors such as bandwidth, channel quality (Line of Sight (LOS), Non-line of Sight (NLOS)). The radio conditions in those cells differ due to factors such as of the considered UEs with respect to BSs (good, bad or excellent coverage, cell edge users, users closer to the cell center, etc) and mobility of users inside the cell. User mobility can be a limitation especially for TDD Massive MIMO performance due to a limit on the time interval during which the channel response must be acquired to update the precoding matrix. We can also observe that as a general rule, lower frequencies (e.g. 800 Mhz plot of Fig. 6) can accommodate more users than higher order frequencies (e.g. 2600 Mhz plot of Fig. 8) (although 1800 Mhz FDD site of Fig. 7 is observed to be deployed in a more densely populated region). This is basically due to higher coverage areas which increase the possibility of the number of users that are served. We can also observe that the number of occurrences of better cell throughput observations of FDD-based MIMO compared to TDD Massive MIMO is higher in Fig. 8, i.e. at high frequencies. The reason is that higher

percentage of UEs are now much closer to BS with LOS and as also pointed out by the authors in [18], FDD performance depends critically on the existence of advantageous propagation conditions, namely, LOS with high Ricean factors.

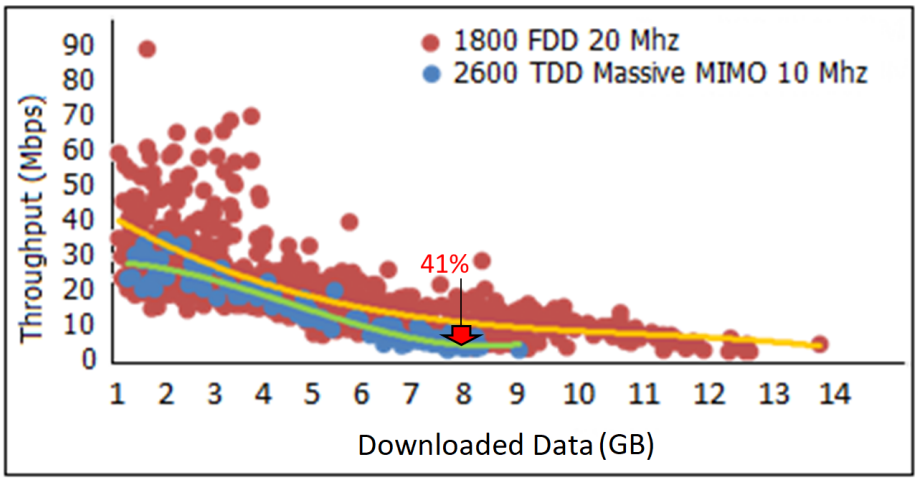

(a)

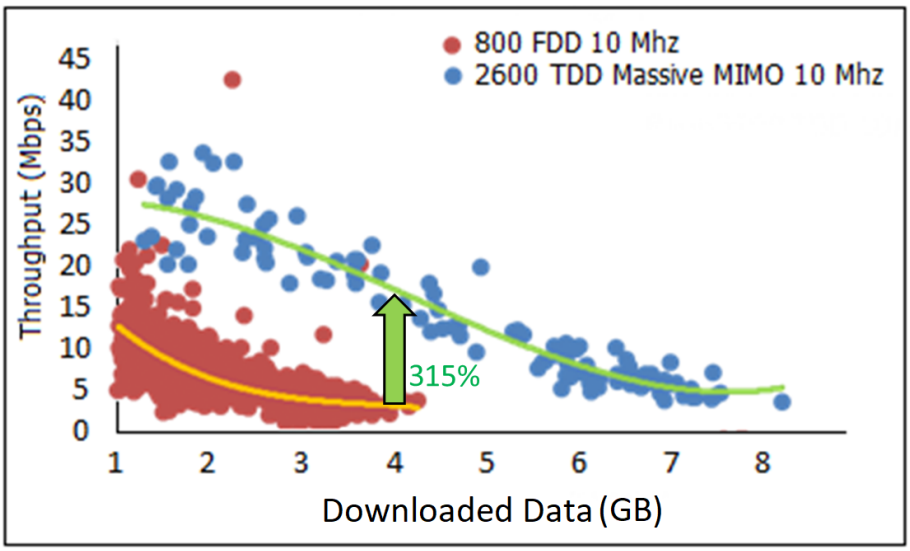

(b)

Figure 9: Co-Site's user throughput versus download data traffic performance comparisons between 2600 TDD massive MIMO and (a) 1800 FDD with 20 Mhz bandwidth (b) 800 FDD 10 Mhz bandwidth.

For FDD MIMO systems, in Fig. 6 the cell throughput has an increasing trend, whereas in both Fig. 7 and Fig. 8 cell throughput values tend to decrease as the number of users increase. We can also observe that Fig. 8 with 1800 Mhz FDD system site has a higher number of users compared to others. On the other hand, TDD massive MIMO systems tend to exhibit best cell throughput results at an optimal number of users (around 60 users) according to fitted regression lines. The results in Fig. 6, Fig. 7 and Fig. 8 have also indicated that increased frequency for FDD system has degraded the system performance. One of the main reasons can be due to the real user behaviour which is different from a controlled test environment setup. Under normal circumstances in a controlled experimental environment, average cell throughput of high and low operating frequencies are expected to be equal under the same bandwidth constraints and number of users. Moreover, in this experimental controlled environment, each user is assigned to download similar sized files, videos, etc. in a continuous manner, which keeps the total cell throughput the same. However in real network environments hence uncontrolled environments, this is not the case. User behaviour is different for each UE and it is not guaranteed that each user will exhibit the same download/upload behaviour compared to controlled environments depending on their choice of service/application usage. Even under the same number of users in the cell, cell throughput can be different and vary as the users can do different access activities (e.g. one user with video and another user can be text messaging) which can also be observed from Fig. 9. The above results signify the validity and importance of performing real-world experiments as the results may depend on several other factors and need to be validated via experimental observations before and after deployments.

In summary, TDD-based massive MIMO has better average cell throughput than FDD based MIMO scheme in all the considered cases above when the user number varies. On the other hand, at high frequencies the performance of FDD MIMO observed to degrade gradually compared to TDD-based massive MIMO scheme.

4.5. TDD Massive MIMO and FDD MIMO User Throughput Performance

Fig. 9(a) shows the scatter plot results of DL user throughput values in Y-axis of co-sites 2.6 GHz TDD-based massive MIMO and 1800 Mhz FDD with 20 Mhz bandwidth and Fig. 9(b) shows the same comparisons between 2600 GHz TDD massive MIMO and 800 Mhz FDD 10 Mhz bandwidth over download data traffic values in X-axis. In both of these figures, green colored line represents the fitted regression line for TDD-based massive MIMO case whereas yellow colored line represents the fitted regression line for FDD-based MIMO case. We can observe that when download data traffic value reaches 8 GB, average user throughput decline of 2600 GHz TDD massive MIMO in comparison with 1800 Mhz FDD is approximately 41% for Fig. 9(a) and when download data traffic value reaches to 4 GB, average user throughput improvement of 2600 GHz TDD massive MIMO in comparison with 800 Mhz FDD is approximately 315% for Fig. 9(b). In Fig. 9, due to higher bandwidth utilization of FDD systems (20 Mhz), higher DL user throughput values are obtained in Fig. 9(a) compared to Fig. 9(b) as expected. Moreover, in this higher bandwidth case, FDD-based MIMO performed better than TDD-based massive MIMO in all download data traffic values.

4.6. Mobile Pair Monitoring

Pairing of UEs means to identify UEs that are separate in space from each other such that each one of them is served by a different grid of beams. In general, the correlation function of beamforming weights of different UEs are checked by the scheduler. If the correlation function is close to zero, those UEs are paired together in a set. Later at each TTI, those UEs in the same set are scheduled together. During experiments, 16 unique data streams or layers are transmitted from the massive MIMO capable BS for geographically scattered UEs to be scheduled together. Therefore at each TTI, 8 paired UEs (each with 2 layers) can be scheduled together.

During our experiments in the DL side, we have observed above described mobile pairing opportunities. In DL, the maximum paired layer reached 14

layers. At each layer, it is observed that different average number PRBs are shared among layers (in which multiple UEs are simultaneously scheduled together) during experiments. Layer-1 is particularly used to measure the number of PRBs that can be paired for MU beamforming and the remaining ones are used to determine PRB pairing for MU beamforming. The remaining layers are used to determine the average number of PRBs successfully paired for MU beamforming. The samples of the measurements for both the number of PRBs that can be paired for MU beamforming at layer 1 and the average number of PRBs successfully paired for MU beamforming at other layers are obtained per second in DL. Later, the average of those samples are used to calculate the corresponding percentage values.

Fig. 10 and Fig. 11 provide values for average number of PRBs successfully paired for MU beamforming measured at each layer (from layer-2 to layer-15) with TDD-based massive MIMO. In Fig. 10 the most number of PRB utilization are concentrated at layers 2, 3 and 4. Depending on the time of the observation, the average number of PRBs that are successfully paired can be up to 17 in the first layer, followed by 11 in layer 2 and 7 in the third layer. We can also observe that the peak values for the number of pairings have occurred around noon over the observation periods (from 23 September 2020 to 25 September 2020). The remaining layers for the pairings of PRBs given in Fig. 11 are observed to be lower than 3. These results indicate that the number of shared PRBs depends on the geographic dispersion of UEs over the cell area of massive MIMO.

4.7. Main Observations and Takeaways

As the network becomes larger and more complicated (with many users, antennas and dense cells), better network planning (i.e. selections of neighbors, locations, etc), coverage, resource, traffic (or capacity) and interference management schemes are required. For this reason, tracking the best optimization parameters and configuration details before and after activation 2.6 GHz TDD-based massive MIMO is important. Deciding on the percentage of UEs to migrate from LTE FDD MIMO to TDD massive MIMO, improving RRC

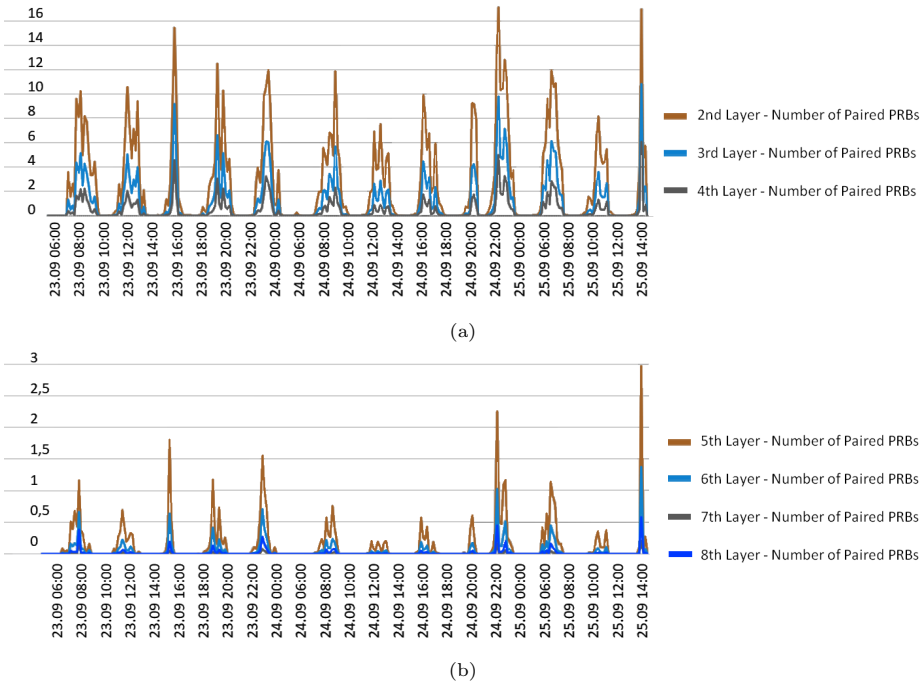

Figure 10: DL Average Pair Layer PRB Success Rates (a) Pair Layers 2 to 4 (b) Pair Layers 5 to 8.

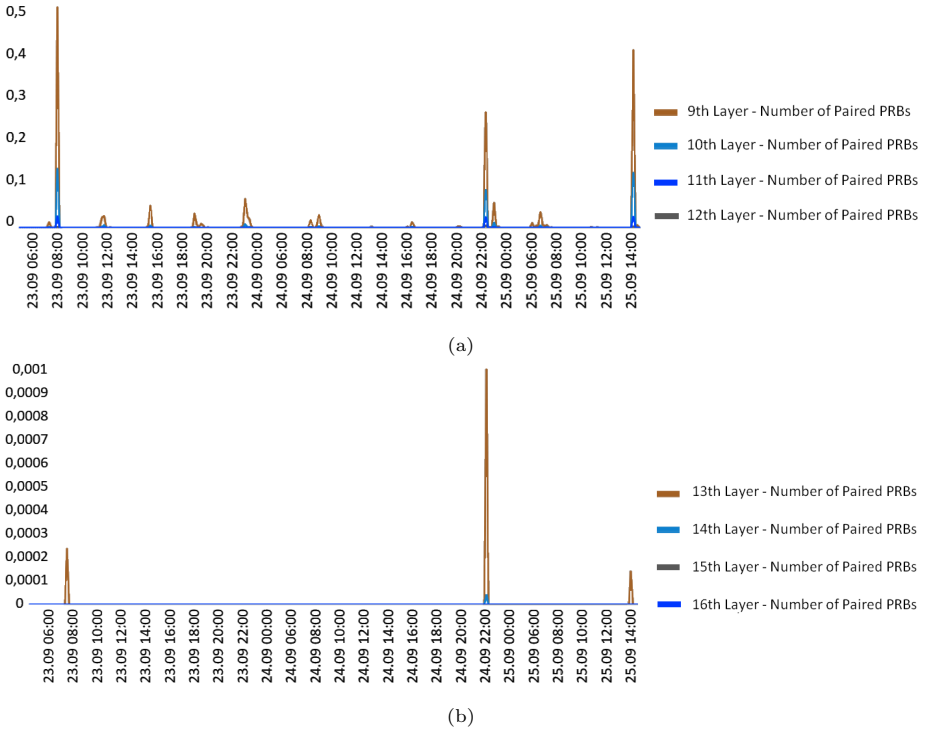

Figure 11: DL Average Pair Layer PRB Success Rates (a) Pair Layers 9 to 12 (db) Pair Layers 13 to 15.

success rate, flexible and dynamic switching options (hard or easy handover) between TMs (e.g. SU-MIMO or massive MIMO) are all other important key performance parameters that need to be optimized depending on the considered use case or scenario (e.g. big event or urban deployments, etc).

One of the main reasons for major improvement of massive MIMO is also due to using TM9 capable devices. These devices are capable of communicating with both SU and massive MIMO transmission modes. TM9-capable devices allow BSs to direct user dedicated beams towards UE with more accurate CSI measurements. This has improved the cell-edge conditions as beamforming allowed to increase the UEs' received signal. Massive MIMO TDD system used in the experiment can also dynamically switch between TM9 and TM4 modes (supports closed loop multiplexing) without special signaling by higher layers. Based on our experimental observations, we also observed that massive MIMO's horizontal beamforming may need to be adjusted to be same with the FDD sector to increase the cell throughput for co-site TDD massive MIMO and FDD MIMO deployments.

During our experiments, the maximum paired layer reached 14 layers in DL using massive MIMO. Under normal circumstances, the number of UEs and the cell throughput have a direct impact on the mobile pairing opportunities. Pairing can free up more PRB resources and Physical Downlink Shared Channel (PDSCH) layers. Therefore, any UEs can benefit from maximum resources from the scheduler. From Fig. 10, we observed that most of the time only the first three layers had high pairing opportunities with low PRB pairings in the remaining layers. This signifies that the UE traffic was somehow observed to be bursty and with a low payload profile. Therefore based on the low number of layers, we can conclude that few occasions for pairings have emerged during the observation period. In case of existence of high traffic volume, scheduling of UEs will be done by the TDD-based massive MIMO deployment system considering them MU candidates. Hence, massive MIMO is very good for cell throughput and capacity if the cell has high traffic. However, if the traffic volume is low, scheduling will be done as SU candidates in a given TTI cycle. Based on

the low observed pairing opportunities over time during our experiments, we can conclude that the total amount of traffic generated by UEs and observed through cell throughput were also not high. Additionally, as the pairing opportunities increase, more UEs can be scheduled together at a given TTI using the same PRBs. This means that the amount of user throughput obtained by each user can be smaller in comparison to full TTI usage by a single UE that can utilize all PRB. During experiments, Fig. 3 has demonstrated the inverse correlation between user throughout and number of DL average paired layers over the observation duration validating this expected behaviour.

At the same time, based on the user throughput scatter plot of Fig. 9, we have observed that LTE 1800 Mhz FDD MIMO at 20 Mhz can yield higher user throughput values in comparison to 2.6 GHz TDD-based massive MIMO at 10 Mhz. This result may indicate two main take-away conclusions: The first one is that the effect of higher bandwidth becomes a more dominant factor in increasing the user throughput than massive MIMO. The second is that the user throughput has also its own limitations due to poor RF conditions even though the advantages brought by massive MIMO features can be in-place (e.g. high number of free PRBs reserved for UEs) and may not help much under those poor RF circumstances. Pilot contamination phenomenon exists in multi-cellular system and is a major challenge for the massive MIMO system implementation. During our experiments, we have not been able to directly observe the effect of pilot contamination in dense user scenarios due to presence of single cell massive MIMO system.

5. Conclusions and Future Work

Massive MIMO is a novel and promising technology that is expected to be a key enabler for 5G and beyond 5G wireless cellular networks by providing high throughput and reliable transmission. In this paper, we investigated the details of a massive MIMO deployment scenario. First, we provided design guidelines and requirements for massive MIMO network deployment, proper acceptance

of KPIs collection and comparisons criteria and gave an overview of the experimental set-up. Second, we compared TDD massive MIMO with FDD MIMO systems in various operating frequencies and different bandwidth for both co-site and separate site scenarios using an operator's network infrastructure in Turkey. We have observed that TDD massive MIMO site's user throughput is observed to be higher than co-site LTE 800M site and the capacity to be higher than same bandwidth other FDD sites. It is also observed that most of the user traffic is transferred from LTE 1800 Mhz co-site after changing the neighbor cell re-selection priority to activate massive MIMO. The maximum paired layer is observed to reach 14 layers in DL. Finally, we provided some important discussions on the outcome of the experimental setup and the involved trade-offs.

As a future direction of our work, more research is needed to introduce new FDD systems into massive MIMO systems and observe their experimental benefits in terms of channel gains, capacity or received power as well as the core KPIs that have been investigated within this paper. Cell-free massive MIMO, which is proposed to overcome the physical limits of cellular networks, is another future direction that demands further research implementation and real-world experimentation. Additionally, future experiments can be designed to compare the performances brought by array gain via increasing the number of BS antennas versus the one brought by using more spectrum bandwidth.

Acknowledgements

This work was partially funded by Spanish MINECO grant TEC2017-88373-R (5G-REFINE) and by Generalitat de Catalunya grant 2017 SGR 1195.

References

[1] Ericsson, Ericsson Mobility Report (June 2020) (White Paper), `https://bit.ly/34MyE9y`, [Online; accessed August-2020] (2019).

[2] T. L. Marzetta, Fundamentals of massive MIMO, Cambridge University Press, 2016.

[3] T. L. Marzetta, Noncooperative cellular wireless with unlimited numbers of base station antennas, IEEE transactions on wireless communications 9 (11) (2010) 3590–3600.

[4] J. Hoydis, C. Hoek, T. Wild, S. ten Brink, Channel measurements for large antenna arrays, in: 2012 International Symposium on Wireless Communication Systems (ISWCS), IEEE, 2012, pp. 811–815.

[5] E. Zeydan, O. Dedeoglu, Y. Turk, Experimental Evaluations of TDD-Based Massive MIMO Deployment for Mobile Network Operators, IEEE Access 8 (2020) 33202–33214.

[6] Qualcomm, Designing 5G NR, `https://www.qualcomm.com/media/documents/files/the-3gpp-release-15-5g-nr-design.pdf`, [Online; accessed October-2020] (2018).

[7] N. Rajatheva, I. Atzeni, E. Bjornson, A. Bourdoux, S. Buzzi, J.-B. Dore, S. Erkucuk, M. Fuentes, K. Guan, Y. Hu, et al., White paper on broadband connectivity in 6G, arXiv preprint arXiv:2004.14247.

[8] S. N. Sur, Massive MIMO for Green Communication, in: Advances in Greener Energy Technologies, Springer, 2020, pp. 833–842.

[9] Y. Okumura, S. Suyama, J. Mashino, K. Muraoka, Recent activities of 5G experimental trials on massive MIMO technologies and 5G system trials toward new services creation, IEICE Transactions on Communications 102 (8) (2019) 1352–1362.

[10] P. Harris, S. Zhang, M. Beach, E. Mellios, A. Nix, S. Armour, A. Doufexi, K. Nieman, N. Kundargi, LOS throughput measurements in real-time with a 128-antenna massive MIMO testbed, in: 2016 IEEE Global Communications Conference (GLOBECOM), IEEE, 2016, pp. 1–7.

[11] J. She, W.-J. Lu, Y. Liu, P.-F. Cui, H.-B. Zhu, An experimental massive MIMO channel matrix model for hand-held scenarios, IEEE Access 7 (2019) 33881–33887.

[12] L. Valle, J. R. Pérez, R. P. Torres, Characterisation of Indoor Massive MIMO Channels Using Ray-Tracing: A Case Study in the 3.2–4.0 GHz 5G Band, Electronics 9 (8) (2020) 1250.

[13] E. P. Simon, J. Farah, P. Laly, Performance evaluation of massive MIMO with beamforming and nonorthogonal multiple access based on practical channel measurements, IEEE Antennas and Wireless Propagation Letters 18 (6) (2019) 1263–1267.

[14] I. Dey, P. S. Rossi, M. M. Butt, N. Marchetti, Experimental Analysis of Wideband Spectrum Sensing Networks using Massive MIMO Testbed, IEEE Transactions on Communications.

[15] A. O. Martinez, J. Ø. Nielsen, E. De Carvalho, P. Popovski, An experimental study of massive MIMO properties in 5G scenarios, IEEE Transactions on Antennas and Propagation 66 (12) (2018) 7206–7215.

[16] R. Chataut, R. Akl, Massive MIMO Systems for 5G and beyond Networks—Overview, Recent Trends, Challenges, and Future Research Direction, Sensors 20 (10) (2020) 2753.

[17] T-Mobile US, Inc., Buckle Up! T-Mobile Achieves Mind-Blowing 5G Speeds with MU-MIMO, `https://t-mo.co/3kgG6OV`, [Online; accessed Sept-2020] (2020).

[18] Flordelis, Jose, et al., Massive MIMO performance—TDD versus FDD: What do measurements say?, IEEE Transactions on Wireless Communications 17 (4) (2018) 2247–2261.

[19] J. Ø. Nielsen, A. Karstensen, P. C. Eggers, E. De Carvalho, G. Steinböck, M. Alm, Precoding for tdd and fdd in measured massive mimo channels, IEEE Access 8 (2020) 193644–193654.

[20] E. Björnson, L. Sanguinetti, H. Wymeersch, J. Hoydis, T. L. Marzetta, Massive MIMO is a reality—What is next?: Five promising research directions for antenna arrays, Digital Signal Processing 94 (2019) 3–20.

[21] B. Panzner, W. Zirwas, S. Dierks, M. Lauridsen, P. Mogensen, K. Pajukoski, D. Miao, Deployment and implementation strategies for massive MIMO in 5G, in: 2014 IEEE Globecom Workshops (GC Wkshps), IEEE, 2014, pp. 346–351.

[22] Rohde & Schwarz, LTE Transmission Modes and Beamforming (White Paper), https://www.rohde-schwarz.com/ae/file/1MA186_2e_LTE_TMs_and_beamforming.pdf, [Online; accessed October-2020] (2015).

[23] TS 38.101-1 v17.0.0, 5G NR; User Equipment (UE) radio transmission and reception; Part 1: Range 1 Standalone, https://portal.3gpp.org/desktopmodules/Specifications/SpecificationDetails.aspx?specificationId=3283, [Online; accessed 5-Feb.-2020] (2020).

[24] TS 38.101-2 v17.0.0, 5G NR; User Equipment (UE) radio transmission and reception; Part 2: Range 2 Standalone, https://www.3gpp.org/ftp//Specs/archive/38_series/38.101-2/, [Online; accessed 7-Feb.-2020] (2020).

[25] E. Ernfors, Radio Stripes: re-thinking mobile networks, https://www.ericsson.com/en/blog/2019/2/radio-stripes, [Online; accessed February-2021] (2019).

[26] E. Björnson, L. Sanguinetti, Scalable cell-free massive mimo systems, IEEE Transactions on Communications 68 (7) (2020) 4247–4261.

[27] T. Zhou, K. Xu, X. Xia, W. Xie, J. Xu, Achievable Rate Optimization for Aerial Intelligent Reflecting Surface-aided Cell-Free Massive MIMO System, IEEE Access.

[28] J. Qiu, K. Xu, X. Xia, Z. Shen, W. Xie, Downlink power optimization for cell-free massive MIMO over spatially correlated Rayleigh fading channels, IEEE Access 8 (2020) 56214–56227.

[29] H. H Yang, Massive MIMO meets small cell, Springer, 2017.

[30] J. Choi, D. J. Love, T. Kim, Trellis-extended codebooks and successive phase adjustment: A path from lte-advanced to fdd massive mimo systems, IEEE Transactions on Wireless Communications 14 (4) (2014) 2007–2016.

[31] C. Qing, B. Cai, Q. Yang, J. Wang, C. Huang, Deep learning for csi feedback based on superimposed coding, IEEE Access 7 (2019) 93723–93733.

[32] S. Dierks, W. Zirwas, M. Jäger, B. Panzner, G. Kramer, MIMO and massive MIMO—Analysis for a local area scenario, in: 2015 23rd European Signal Processing Conference (EUSIPCO), IEEE, 2015, pp. 2451–2455.

[33] D. C. Araújo, T. Maksymyuk, A. L. de Almeida, T. Maciel, J. C. Mota, M. Jo, Massive MIMO: survey and future research topics, Iet Communications 10 (15) (2016) 1938–1946.

[34] E. Björnson, J. Hoydis, L. Sanguinetti, et al., Massive MIMO networks: Spectral, energy, and hardware efficiency, Foundations and Trends® in Signal Processing 11 (3-4) (2017) 154–655.

[35] 3GPP TS 36.213 version 12.3.0. 3rd Generation Partnership Project Technical Specification, LTE Evolved Universal Terrestrial Radio Access (E-UTRA) Physical layer procedures (Release 12) (2014).

[36] Y. Türk, E. Zeydan, On Performance Analysis of Multi-Operator RAN Sharing for Mobile Network Operators, Turkish Journal of Electrical Engineering & Computer Sciences (accepted).

[37] A. Yildirim, E. Zeydan, I. O. Yigit, A statistical comparative performance analysis of mobile network operators, Wireless Networks 26 (2) (2020) 1105–1124.

[38] 3GPP TS 38.214 V16.4.0, NR; Physical layer procedures for data (Release 16, `https://www.3gpp.org/ftp//Specs/archive/38_series/38.214/`, [Online; accessed 7-Feb.-2020] (2020).

Vitae

Engin Zeydan received his Ph.D. degree in February 2011 from the Department of Electrical and Computer Engineering at Stevens Institute of Technology, Hoboken, NJ, USA. Previously, he received his M.Sc. and B.Sc. degrees from the Department of Electrical and Electronics Engineering at Middle East Technical University, Ankara, Turkey, in 2006 and 2004, respectively. Dr. Zeydan has worked as an R&D engineer for Avea, a mobile operator in Turkey, between 2011 and 2016. He was with Turk Telekom Labs working as a Senior R&D Engineer between 2016 and 2018. He was also a part-time instructor at Electrical and Electronics Engineering department of Ozyegin University between 2015 to 2018. He is currently with the Communication Networks Division of the Centre Tecnològic de Telecomunicacions de Catalunya (CTTC) working as a Senior Researcher. He received the Best Paper Award from the Network of Future Conference in 2017. His research interests are in the areas of telecommunications and big data networking.

Omer Dedeoglu received his BS degree in Electrical&Electronics Engineering from Bilkent University in 2001 and MS degree in Electrical&Computer Engineering from New Mexico University in 2003. He worked for R&D projects and made Radio NW investment plans at Turkcell for about 6 years. Since 2011, Omer Dedeoglu has been working at Turk Telekom as radio network planning expert& manager.

Yekta Turk received his Ph.D. degree in 2018 from the Department of Computer Engineering at Maltepe University, Istanbul,Turkey Previously, he received his M.Sc. degree from in Telecommunications and Computer Networks from the George Washington University, DC, USA, in 2007 and B.Sc. degree in Electrics and Electronics Engineering from Anadolu University, Turkey, in 2005. He has worked in fixed and mobile network operators for 11 years. He is

765 a mobile network architect based in Istanbul, Turkey. His research interests are in the area of mobile radio telecommunications and computer networks.